Supplementary Information and Methods

Dissection of single-cell landscapes for the development of chimeric antigen receptor T cells in Hodgkin lymphoma

Adrian Gottschlich[1,2,3,4*], Ruth Grünmeier[2*], Gordon Victor Hoffmann[2*], Sayantan Nandi[2*], Vladyslav Kavaka[5,6], Philipp Jie Müller[2], Jakob Jobst[2], Arman Öner[2], Rainer Kaiser[7,8], Jan Gärtig[2], Ignazio Piseddu[2,3,9], Stephanie Frenz-Wiessner[10,11], Savannah D. Fairley[10,12], Heiko Schulz[13], Veronika Igl[2], Thomas Alexander Janert[2], Lea di Fina[7], Maité Mulkers[7], Moritz Thomas[14,15], Daria Briukhovetska[2], Donjetë Simnica[2], Emanuele Carlini[2], Christina Angeliki Tsiverioti[2], Marcel P. Trefny[2], Theo Lorenzini[2], Florian Märkl[2], Pedro Mesquita[2] , Ruben Brabenec[2,14], Thaddäus Strzalkowski[2], Sophia Stock[1,2,3,4], Stefanos Michaelides[2], Johannes Hellmuth[1], Martin Thelen[16,17], Sarah Reinke[18], Wolfram Klapper[18], Pascal Francois Gelebart[19,20], Leo Nicolai[7,8], Carsten Marr[14], Eduardo Beltrán[5,6,21], Remco T. A. Megens[12,22,23], Christoph Klein[10,11,24], Fanny Baran-Marszak[25,26], Andreas Rosenwald[27,28], Michael von Bergwelt-Baildon[1,3,4], Paul J Bröckelmann[29,30], Stefan Endres[2,4,31] and Sebastian Kobold[2,4,31]

[1] Department of Medicine III, LMU University Hospital, LMU Munich, Munich, Germany.
[2] Division of Clinical Pharmacology, LMU University Hospital, LMU Munich, Munich, Germany.
[3] Bavarian Cancer Research Center (BZKF), Munich, Germany.
[4] German Cancer Consortium (DKTK), Partner Site Munich, Germany.
[5] Institute of Clinical Neuroimmunology, LMU University Hospital, LMU Munich, Munich, Germany.
[6] Biomedical Center (BMC), Faculty of Medicine, LMU Munich, Martinsried, Germany.
[7] Department of Medicine I, LMU University Hospital, LMU Munich, Munich, Germany.
[8] DZHK (German Center for Cardiovascular Research), partner site Munich Heart Alliance, Munich, Germany.
[9] Department of Medicine II, LMU University Hospital, LMU Munich, Munich, Germany.
[10] Department of Pediatrics, Dr. von Hauner Children's Hospital, LMU University Hospital, LMU Munich, Munich, Germany.
[11] German Center for Child and Adolescent Health, Partner Site Munich, Munich, Germany.
[12] Institute of Cardiovascular Prevention (IPEK), Ludwig-Maximilians-University Munich, Munich, Germany.
[13] Institute of Pathology, Faculty of Medicine, LMU Munich, Munich, Germany.
[14] Institute of AI for Health, Helmholtz Zentrum München - German Research Center for Environmental Health Neuherberg, Germany.
[15] School of Life Sciences Weihenstephan, Technical University of Munich, Freising, Germany.
[16] Department of General, Visceral, Cancer and Transplantation Surgery, University of Cologne, Faculty of Medicine and University Hospital Cologne, Cologne, Germany.
[17] Center for Molecular Medicine Cologne, University of Cologne, Faculty of Medicine and University Hospital Cologne, Cologne, Germany.
[18] Department of Pathology, Hematopathology Section, University Hospital Schleswig-Holstein, Campus Kiel, Kiel, Germany.
[19] Department of Clinical Science, University of Bergen, Bergen, Norway.
[20] Department of Hematology, Haukeland University Hospital, Bergen, Norway.
[21] Munich Cluster for Systems Neurology (SyNergy), Munich, Germany.
[22] Department of Biomedical Engineering (BME), Cardiovascular Research Institute Maastricht (CARIM), Maastricht University Medical Centre, Maastricht, The Netherlands.
[23] German Center for Cardiovascular Research (DZHK), Partner Site Munich Heart Alliance, Munich, Germany.
[24] Gene Center, LMU Munich, Munich, Germany.
[25] INSERM U978, University of Paris 13, Bobigny, France.
[26] Service d'Hématologie Biologique, Hôpitaux Universitaire Paris Seine Saint Denis (HUPSSD), Hôpital Avicenne, Université Sorbonne Paris Nord Bobigny, France.
[27] Comprehensive Cancer Center Mainfranken, University Hospital Würzburg, Würzburg, Germany.
[28] Institute of Pathology, University of Würzburg, Würzburg, Germany.
[29] University of Cologne, Faculty of Medicine and University Hospital of Cologne, Department I of Internal Medicine, Center for Integrated Oncology Aachen Bonn Cologne Düsseldorf (CIO ABCD) and German Hodgkin Study Group (GHSG), Cologne, Germany.
[30] Max Planck Institute for Biology of Ageing, Cologne, Germany.
[31] Einheit für Klinische Pharmakologie (EKLiP), Helmholtz Zentrum München - German Research Center for Environmental Health Neuherberg, Germany.

* these authors contributed equally

Methods

Microarray analysis

Deposited microarray data from GSE 12453[1] and GSE20011 were analyzed using the publicly available R script from Mark Dunning (https://sbc.shef.ac.uk/geo_tutorial/tutorial.nb.html) with minor adjustments. Briefly, the series matrix file was loaded using the getGEO function of the GEOquery library. The input data were log2 transformed. Subsequently, only genes were kept that are expressed in more than 2 samples. The groups were defined according to the column source_name_ch1 of the phenotypic data of the series matrix. Samples from naïve B cells and memory B cells were grouped as "PB B cells" and centrocytes, centroblasts as well as plasma cells were grouped into "germinal center cells". Using the function model.matrix from the limma package a design matrix was created. The expression level of each probe in each group was estimated by using the limma function lmFit including the arrayWeights parameter. Finally, we performed the differential analysis by defining the contrast between the groups of interest using makeContrasts.

Single-cell analysis

To assess the composition of the cHL microenvironment, we analyzed single-cell RNA-sequencing data of 22 cHL and 5 reactive lymph nodes (RLN) samples (EGAS00001005541[2]). The Seurat R package (Version 4.0.3) was used for the initial quality control (cells with more than 15% of mitochondrial genes fraction and/or fewer than 200 genes/cell were discarded) and log-normalization of the raw counts data of 127,686 cells. Subsequently, the object was split by the sample of origin and integrated with the reciprocal Principal Component Analysis (PCA) method[3]. For the integration anchors selection, the highly variable features were detected within each sample by the FindVariableFeatures function of the Seurat package with the "vst" selection method. After successful integration, the expression data was scaled with the number of RNA counts and percentage of mitochondrial genes per cell for the subsequent PCA calculation. Based on the first 30 dimensions, we applied an unbiased k-nearest neighbors and cluster identification with 0.8 resolution with the FindNeighbors and FindClusters functions in Seurat. In the next step, we calculated the two-dimensional uniform manifold approximation and projection (UMAP) to visualize the cell embedding. For cell annotations, we performed the differential gene expression (DGE) comparison of each cell cluster against the rest of the cells with the FindAllMarkers function and filtering of the genes according to the p-adjusted threshold of 0.05. All DGE analyses performed in this study used the Wilcoxon test with subsequent Bonferroni p-value adjustment. The CellCycleScoring function of the Seurat R package was used for cell cycle state identification. The visualization plots were computed with the ggplot2 (Version 3.4.0) and Seurat.

In the next step, we assessed the distribution of the clusters between the cHL and RLN samples. For this purpose, the number of cells within each cluster was normalized by the total cell count per diagnosis. The fold changes were calculated by dividing the fraction of HL-cell by the RLN-derived cells with subsequent log2 transformation.

To evaluate the activity of various activatory and inhibitory immunological axes [4], we performed a DGE analysis between the HL and RLN samples consecutively within each cluster by running the FindMarkers function. This approach enabled us to avoid the cell/subset- and distribution-related bias during the markers identification. The significantly upregulated genes were retrieved according to the p-adjusted threshold. Subsequently, we selected only the markers present within the activatory or inhibitory panel with the following visualization of the log2 fold-changes results.

Generation of a single-cell atlas for off-tumor expression screening

All preprocessing and analysis steps of scRNA-Seq data analysis for off-tumor target screening were run in python 3 using Scanpy v.1.8.2+[5] and anndata v.0.7.8+[6] except stated otherwise. All scRNA-Seq figures were plotted using matplotlib and seaborn.

Single-cell transcriptomic datasets were obtained either via sfaira[7], cellxgene (https://cellxgene.cziscience.com/) or from various depositories listed in the respective original studies. A detailed description of the datasets used can be found in **Extended Data Figure 1C**.

For each dataset, low-quality cells were removed based on total UMI count, gene distributions and fraction of mitochondria-encoded genes per sample after visual inspection (see provided Notebook). Genes that were detected in less than 20 cells were excluded for further analysis. Normalization of UMI counts of each cell was carried out using the implemented R-based SCRAN algorithm[8, 9]. Briefly, size factors were estimated upon clustering the data using the Louvain algorithm implemented in Scanpy (tl.louvain) before running ComputeSumFactors with min.mean = 0.1. Size factors were then used for cell normalization. Finally, the data was log-transformed (log(count+1)). Cell annotation labels were provided by the authors of the respective study and were carefully inspected and harmonized between datasets upon close inspection of marker gene expression. The normalized cell x gene matrix was then used for plotting mean expression values across cell types (see provided Notebook).

Cell lines

Human cHL cell lines L-428, L-540 and KM-H2 or Nalm-6 acute lymphomblastic leukemia (ALL) cell line were purchased from ATCC (USA). The murine J774A.1 cell line was kindly provided by P. Düwell (Institute of Innate Immunity, University Hospital Bonn). All cells were transduced with a pCDH-EF1a-eFly-eGFP plasmid[10] purchased from addgene (plasmid #104834, deposited by I. Jeremias) and enhanced green-fluorescent protein (eGFP) positive cells were sorted with a BD FACSAria™ III Cell Sorter. STR profiling was carried out at the Institute for Forensic Medicine of the LMU Munich to ensure the correct origin of all cell lines. Mycoplasma contamination was excluded by regular testing for mycoplasma using polymerase chain reaction (PCR). All cell lines were cultured in RPMI containing 20 % FBS, 2 mM L-Glutamine, 100 U/ml penicillin and 100 µg/ml streptomycin. All cells were grown at 37°C in a humidified incubator with 5 % CO_2. Cells were stored at -80°C or in liquid nitrogen after addition of freezing medium (90 % FBS and 10 % DMSO).

Animal experiments

All animal experiments were approved by the local regulatory agency (Regierung von Oberbayern, ROB). Following written approval, experiments were performed following the regulations determined by the ROB and in respect of the general guidelines for animal experimentation and animal ethics. All mice were housed in specific-pathogen-free facilities. Mice (C57Bl/6, NOD.Cg-Prkdc^{scid} Il2rg$^{tm1WjI/SzJ)}$ were purchased from Janvier (St Berthevin, France), Charles River Laboratories (Sulzfeld, Germany) or bred at our facilities.

cHL xenograft models (L-428, L-540) were intravenously (i.v.) injected into NSG mice at the indicated cell numbers. As described, all tumor cells were transduced with a pCDH-EF1a-eFly-eGFP plasmid and tumor progression was monitored using bioluminescence imaging (BLI, *In vivo* Imaging System Platform Lumina X5 (IVIS, PerkinElmer, USA)). BLI was performed after intraperitoneal injection (i.p.) of BLI substrate (Xenolight D Luciferin potassium salt, Perkin Elmer, USA). For narcosis, mice were anesthetized using an isoflurane-oxygen mixture (1.5 – 2.8 %). T cells were transferred following successful tumor engraftment measured by BLI. Time of adoptive T cell transfer (ACT) and number of transferred T cells are indicated in each respective experimental summary scheme. For all BLI images, the red cross indicates that mice reached the pre-defined abortion criteria and died due to tumor-related causes. Mice that had to be removed due to non-tumor-related toxicities (e.g. Graft-versus-host-disease) were censored in Kaplan-Meier curves.

For humanized mouse experiments, tumor-bearing mice were injected i.v. with 20 million PBMC derived from healthy human donors. Antibody treatment was conducted as depicted in the respective figures. All antibodies were injected i.p.. For humanized mouse experiments, 150 µg ultra-leaf anti-human CD86 antibody (clone IT2.2), anti-mouse IgG2a isotype control antibody or Nivolumab (anti-PD-1 antibody) was injected per mouse, every two to three day until each mouse received a maximum of 600 µg. Experiments leveraging immunocompetent C57Bl/6 mice were conducted as illustrated in the respective figures. For antibody-blocking experiments 200 µg of anti-mouse CD86 antibody (clone: GL-1) or rat IgG2a isotype control were injected on day -7 and day -4 as indicated. For CAR T cell experiments, mice were lymphodepleted either with 3,5 Gy or 5,5 Gy total body irradiation (TBI).

To assess *in vivo* T cell proliferation and to perform tumor site enrichment analysis, transferred T cells were double transduced with the respective CAR construct and a pmp71-teLuc-F2A-mCherry plasmid (sequence obtained from pcDNA3-teLuc c-myc plasmid; plasmid #100026, deposited by H. Ai)[11]. TeLuc substrate DTZ was purchased from MedChemExpress and dissolved according to manufacture's instruction.

A detailed description of the vaccination experiments and the polymicrobial sepsis model is provided below.

Vaccination experiment

C57BL/6J mice were s.c. treated with a vaccine consisting of 50 µg OVA protein (InvivoGen), 10 µg ODN1826 (InvivoGen) and 2 mg Imject Alum (ThermoFisher) twice in an interval of one week. One week after the second vaccination, blood and spleen were isolated from mice and single-cell suspensions were generated as described above. Blood-derived cells and splenocytes were stained with anti-CD3-FITC (clone: 17A2, BioLegend), anti-CD8-APC (clone: 53.6-7, BioLegend), Zombie Violet Fixable Viablity Kit (BioLegend) and H-2kB-SIINFEKL-PE-pentamer (Proimmune) and analyzed by flow cytometry. Additionally, 2 x 10^6 splenocytes from each mouse were seeded in a 96-U-well plate and stimulated with 1 µg SIINFEKL protein (InvivoGen) or left unstimulated. The plate was incubated at 37°C for 1 h and subsequently, cells were treated with Brefeldin A (BioLegend). After further incubation at 37°C for 4 h, cells were extracellularly stained with anti-CD3-FITC (clone: 17A2, BioLegend), anti-CD8-APC (clone: 53.6-7, BioLegend) and Zombie Violet Fixable Viability Kit (BioLegend). Upon fixation and permeabilization with FoxP3 staining kit (ThermoFisher) according to manufacturer`s instructions, cells were intracellularly stained with anti-IFNγ-PE (clone: XMG1.2, BioLegend) and analyzed by flow cytometry.

Polymicrobial peritonitis through cecal slurry injection

We used peritoneal cecal slurry (CS) injections to induce a clinically relevant and reproducible model of sepsis following previously established protocols[12]. CS was prepared by collecting the cecal content of young, untreated C57BL/6J wild-type mice, followed by filtering steps and mixing with glycerol before cryopreservation. CS stocks collected and pooled from the same mice were used throughout all experiments shown in this study. Following pre-treatment with either i.p. antibody injection or TBI and i.v. perfusion of CAR T cells, female C57BL/6J mice aged 8-10 weeks were injected with 200 µl of CS. Mice were incubated and scored over 6 hours. If mice did not develop sepsis-associated symptoms (that is, an overall score of <1 at 6 hours), intestinal rather than peritoneal injection was assumed, and mice were excluded from downstream assays. Hereafter, mice were anaesthetized with isoflurane, cheeks were disinfected, and blood was harvested through puncture of the facial veins, followed by sacrifice through cervical dislocation. To assess local immune cell recruitment to the peritoneal cavity, 10 ml PBS containing 0.25% BSA and 5 mM EDTA were intraperitoneally injected. Following injection, abdominal massage was performed to ensure equal distribution of the fluid throughout the peritoneal cavity. Hereafter, the lavage fluid was collected through a puncture with a 20G needle. The lavage samples were discarded if less than 50% of the injected volume (i.e. 5 ml) were retrieved or if the puncture had caused significant hemorrhage, leading to blood contamination of the lavage fluid. Peritoneal lavage samples were then pelleted through centrifugation, followed by erylysis (FACS™ Lysing Solution, BD) and antigen blockade using anti-mouse Fc block (BioLegend). Leukocyte populations were then stained using fluorescent antibodies and viability stains, followed by additional centrifugation and filtering steps.

Assessment of colony-forming units

To assess bacterial containment in experimental groups, 50 µl of whole blood (undiluted and diluted 1:20 in sterile PBS) were evenly distributed on LB agar plates. Plates were dried, turned upside down and incubated over night at 37°C, 5% CO2. Formed colonies were counted after 16 hours of incubation and normalized to CFUs/µl.

Flow cytometry

Flow cytometric analysis was performed using a LSRFortessa™ II, a Beckman Coulter CytoFLEX LX or a Cytek™ Aurora spectral analyzer. To carry out flow cytometric analysis, cells were centrifuged at 200 to 400 g for 5 min at 4°C in a pre-cooled centrifuge and washed twice with PBS. Before all staining, Fc receptors were blocked using a human TruStain FcX™ (2.5 µl per well) and dead cells were excluded using staining with a fixable viability dye (eFluor™ 780, eBioscience, USA) for at least 10 min at room temperature in the dark or 30 min at 4 °C. Cells were again washed twice with PBS and then stained with the respective antibodies for 30 min at 4 °C. Cell counts were normalized by adding 2.5 µl of CountBright™ Absolute Counting Beads (Thermo Fisher Scientific, USA) into each well or tube.

Following antibodies were used to stain for target gene expression on cHL cell lines:

Anti-CD30 (clone: BY88), anti-CD86 (clone: IT2.2), anti-CD80 (clone: 2D10), anti-PD-L1 (clone: 29E.2a3), anti-CD14 (clone: HCD14), anti-CD90 (clone: 5E10), anti-CD163 (clone: GH1/61), anti-CD213a (clone: SS12B) and anti-FPR1 (clone: W15086B). Mouse IgG1 isotype (clone: MOPC-21) and Mouse IgG2a (MOPC-173) antibodies were used as controls.

For PBMC blocking assays, humanized mouse models and BMO models staining included these antibodies: anti-CD45 (clone: HI30), Anti-CD30 (clone: BY88), anti-CD86 (clone: IT2.2), anti-CD80 (clone: 2D10), anti-PD-L1 (clone: 29E.2a3), anti-CD14 (clone: HCD14), anti-CD3 (clone: UCHT1, HIT3a), anti-CD4 (clone: OKT4) and anti-CD8 (SK1, HIT8aa), anti-PD-L2 (clone: MIH18), anti-CD28 (clone: CD28.2), anti-CTLA-4 (clone: L3D10). For blocking assays with PBMC and BMO before platting the assay, PBMC were stained with a CellTrace™ Far Red Cell Proliferation according to manufacture's instruction.

Transduction efficiency was assessed with anti-c-myc FITC (clone SH1-26E7.1.6; Miltenyi Biotec, Germany). Following antibodies were used for co-cultures of CAR T cells and tumor cells or CAR T cells and macrophages: anti-CD3 (clone: UCHT1, HIT3a) anti-CD4 (clone: OKT4) and anti-CD8 (SK1, HIT8aa) antibodies were used to gate on T cells. Anti-mouse/human CD11b (clone: M1/70) antibody was used to gate on macrophages. Anti-human CD69 (clone: FN50) and anti-PD-1 (clone: EH12.2H7) antibodies were used to assess T cell activation. *In vitro*-polarized macrophages were characterized using multicolor flow cytometry panel including these antibodies: Anti-CD11b (clone: M1/70), anti-CD163 (clone: GHI/61) and anti-CD206 (clone: 15-2).

Anti-mouse CD86 antibody (clone: GL-1) was used to stain for expression of mCD86 protein.

All antibodies were purchased from BioLegend, USA, if not otherwise indicated.
Before staining for GzmB and Perforin, GolgiPlug and GolgiStop protein trafficking inhibitors were added to the co-culture wells. After 12 hours, cells were harvested, washed with PBS and extracellularly stained as described above. Then intracellular FACS staining was performed using established protocols by the provider (Fixation/ Permeabilization Kit, BD Bioscience, USA).
The absolute molecule count of target antigens was determined using BD Biosciences™ Quantibrite™ Phycoerythrin (PE)-Beads according to manufacture's instruction. Stainings were either carried out using primary PE-coupled antibodies or stained with a primary antibody followed by staining with PE anti-mouse IgG1 (clone RMG1-1, BioLegend USA) or PE anti-mouse IgG2b (clone RMG2b-1, BioLegend USA).
Delta MFI = MFI of sample stained with target antibody - MFI of sample stained with isotype control.

Generation of CAR constructs

CAR constructs were either cloned using conventional protocols or designed *in silico* and obtained from commercial vendors (Twist Bioscience, USA). The configurations of the generated CARs are illustrated in **Figure 4A** and **Extended Figure 8A**, respectively. The human anti-CD86 single-chain variable fragment was derived from a patented sequence of an anti-CD86-binding antibody (clone 3D1; Patent Number: US2002/0176855A1). The murine anti-CD86 single-chain variable fragment was derived of clone GL-1.
The murine anti-EpCAM CAR has extensively been described[13, 14]. Anti-CD19 CAR T cells were designed based on the patented anti-CD19-CAR-FMC63-28Z CAR T cells (WO 2015/187528 A1). Anti-CD30 CARs were designed from patented anti-CD30 CAR T cells currently used in clinical trials (WO 2017/066122 A1; (ClinicalTrials.gov Identifier: NCT03049449)). All CAR constructs included a c-myc tag to enable CAR detection.

Retroviral human T cell transduction

Retroviral transduction was carried out using established described protocols comprehensively described elsewhere[13-16]. In brief, CAR constructs were expressed in stable retroviral-producing cell lines 293Vec-Galv, 293Vec-RD114 and 293-Vec-Eco[17]. Density centrifugation was used to isolate human T cells from healthy donors after informed consent. Cells were either enriched for T cells using magnetic-associated cell sorting (MACS, CD3 microbeads, Miltenyi Biotec, Germany) or directly stimulated with human T-Activator CD3/CD28 Dynabeads® (Life Technologies, Darmstadt, Germany) in human T cell medium containing 2.5 % human serum, 2 mM L-Glutamine, 100 U/ml penicillin and 100 µg/ml streptomycin, 1 % Sodium Pyruvate and 1 % non-essential amino acids supplemented with recombinant human IL-2 (PeproTech, USA, Novartis, Switzerland) and IL-15 (PeproTech USA, Miltenyi Biotec Germany). Cells were used for retroviral transduction after 48 hours of activation. T cell transduction was then carried out as described[13, 14, 16, 18].

Murine transductions were carried out as previously described [13, 14].
For all functional assays, transduction efficiencies of CAR T cells were adjusted to the lowest measured transduction efficiency with non-transduced T cells of the same donor to ensure similar rates of CAR expression across different CAR conditions.

NanoString profiling

NanoString gene expression profiling was performed on primary HL specimens from patients enrolled in the prospective investigator-initiated German Hodgkin Study Group (GHSG) randomized multicenter phase II NIVAHL trial (NCT03004833). In the NIVAHL trial, early-stage unfavorable cHL patients (n = 109, of which n = 95 with evaluable NanoString data) were either randomized to receive four cycles of a treatment consisting of concomitant anti-PD-1 immunotherapies (Nivolumab) with chemotherapy (N-AVD, group A) or a sequential therapy regimen with four cycles nivolumab, two cycles of N-AVD and two cycles of AVD (group B). Both treatment arms received consolidative 30 Gy involved-site radiotherapy. The trial results, including methodology, patient characteristics, safety and efficacy have been published[19, 20]. All patients reported within this manuscript provided written informed consent in accordance with the Declaration of Helsinki. The data analyses of the NIVAHL study samples were processed using the NanoString platform. The data was decoded according to the developer protocol using nSolver Analysis Software 4.0.

Immunohistochemistry

CD30 staining was performed on the automated immunohistochemistry system Ventana BenchMark Ultra Plus (Roche Diagnostics, Rotkreuz, Switzerland). Antigen retrieval was performed using CC1 Antigen Retrieval buffer (Roche Diagnostics, Rotkreuz, Switzerland). Anti-CD30 primary antibody (mouse, monoclonal, clone: Ber-H2; Epredia™ Lab Vision™, Thermo Fisher Scientific, Waltham, MA, USA) at 1:25 dilution and 28 minutes incubation time. Antibody detection and visualization were achieved using the ultraView Universal DAB Detection Kit and counterstained with hematoxylin and bluing solution (Roche Diagnostics, Rotkreuz, Switzerland).
For CD86 immunohistochemistry, heat-induced epitope retrieval was performed with citrate buffer (pH 7.0; Diagnostic Bio Systems, Pleasanton, CA, USA; Cat. No. K036). Afterwards, slides were incubated for 60 min at room temperature using anti-CD86 monoclonal antibody (Rabbit, monoclonal, clone: E2G8P; Cell Signaling, Danvers, MA, USA; Cat. No. #91882) at 1:70 dilution. Staining was detected using MACH 3 Rabbit HRP Polymer detection kit (Zytomed Systems, Berlin, Germany; Cat. No. M3R531) and visualized using DAB+ (Agilent Technologies, Santa Clara, CA, USA; Cat. No. K3468). Counterstaining was performed with Gill`s Formula hematoxylin (Vector Laboratories, Newark, CA, USA; Cat. No. H-3401).
Image Quantification was performed with QuPath. After importing the images into the software, first staining vectors were set. Ten rectangle annotations in corresponding regions of the H&E stained, the

CD86 IHC and the CD30 IHC slide were chosen. Cell detection command was used to identify cells based on hematoxylin optical density inside the rectangle annotations. Based on the detected cells. We interactively trained a tumor-non-tumor cell object classifier and IHC positive and IHC negative cell classifier with manual annotation tools. By combining both classifiers, we could classify cells into tumor cells or non-tumor cells as well as IHC positive or negative cells.

Chip Cytometry

Fixed-paraffin-embedded cHL specimens were obtained after written informed consent in regulation of the Declaration of Helsinki. The use of the samples was approved by the Institutional Review Board of the Julius-Maximilians-University, Würzburg. Achieved samples were rehydrated in a rehydration row. Heat-mediated epitope retrieval was carried out using Antigen Retrieval EDTA Buffer pH = 9 (Abcam, ab93684). Slides were then permeabilized in 0,1% Triton X-100 solution for 15 minutes. Slides were transferred onto ZellSafe™ chips (Canopy Biosciences) and stored at 2 - 8°C. Before staining, chips were blocked with 5% donkey serum in PBS for 2 hours at room temperature. CD86 staining was performed using a primary anti-human CD86 antibody (Cell Signaling Technology, #91882, 1:100). Slides were stained overnight at 2 - 8°C. Then, PE-conjugated secondary anti-rabbit antibody (Jackson ImmunoResearch, 711-116-152, 1:100) was used for 2 hours at room temperature for antibody detection. Following photobleaching for 30 seconds, the primary anti-CD20 antibody (Novus Biologicals, NBP2-44743, 1:100) was applied overnight at 2 - 8°C. PE-conjugated secondary anti-mouse antibody (Jackson ImmunoResearch, 715-116-150, 1:100) was applied for 2 hours at room temperature for antibody detection. Cell nuclei were stained for 5 minutes at room temperature using DNA-Hoechst (Invitrogen, 62249, 1:50.000). Chemical bleaching was performed according to published protocols[21]. CD30 staining was carried out using a PE-conjugated (PE Conjugation Kit, Abcam, ab102918) primary anti-human CD30 antibody (Abcam, ab23766, 1:80/1:300) for 2 hours at room temperature. All stainings were acquired on a Zeiss microscope (Zeiss Axio Observer 7) with a halogen lamp for excitation of the used fluorophores (Zeiss HBO 100 Microscope Illuminator).

PBMC-cHL co-cultures with CD86-blocking antibodies

For blocking assays 100.000 PBMC were co-cultured with 50.000 cHL tumor cells in human T cell medium for 5 days and treated with 10 µg ultra-leaf anti-CD86 antibody (clone IT2.2) or mouse IgG2a isotype control (clone: MOPC-21). Antibody concentrations were titrated with flow cytometry before functional assays and revealed near complete absence of CD86 expression with 10 µg and 1 µg. After 5 days, cells were collected as previously described and analysed with flow cytometry.

iPSC cell line and maintenance

The human iPSC line (HMGU1, hPSCreg IFSi001-A) was provided by the iPSC Core Facility, Institute of Stem Cell Research, Helmholtz Center Munich. Human iPSCs were cultured under feeder-free

conditions on Geltrex-coated (Gibco) plates in mTeSRplus medium (STEMCELL Technologies), with medium changes every other day, passaging with ReLeSR (STEMCELL Technologies) every 4–5 days, and routine testing for mycoplasma infections.

Bone marrow organoid differentiation

Bone marrow organoids (BMOs) were differentiated as previously described by Frenz-Wiessner et. al.[22] Briefly, on day -3, iPSCs were dissociated into single cells using Accutase (Gibco), collected, and resuspended in aggregation medium (KnockOut DMEM/F12 supplemented with KnockOut Serum Replacement, penicillin-streptomycin L-glutamine, ß-mercaptoethanol, and nonessential amino acids) containing ROCK inhibitor to form embryoid bodies (EBs). After 24 hours, the medium was replaced with fresh aggregation medium without ROCK inhibitor, and mesoderm induction was initiated on day 0 using mTeSRplus with BMP4, CHIR99021, and VEGF. All cytokines were purchased from StemCell Technologies. On day 2, the medium was switched to Essential 6 (Gibco) with VEGF, bFGF, SCF, and SB431542. On day 4, EBs were embedded in a collagen I (ibidi)-Matrigel (Corning) mixture for further development in Stempro-34 medium (Gibco) with VEGF, bFGF, SCF, and SB431542. The embedded EBs were then cultured in Stempro medium containing IL-3, Flt-3L, TPO, VEGF, and SCF, with medium changes on days 6, 8, and 10. On day 10, sprouted EBs were extracted from the 3D matrix and transferred to a low-attachment plate for continued culture in a cytokine-supplemented medium, with half the medium refreshed every 3–4 days until full maturation by day 17. BMOs were subsequently used for co-culture experiments.

Complex bone marrow organoid and PBMC co-cultures

For co-culture experiments, BMO were grown as described above. After successful differentiation, 200.000 PBMC were stained with CellTrace™ Far Red Cell Proliferation according to manufacture's instruction. Cells were then co-cultured with 50.000 cHL tumor cells in human T cell medium for 5 days and treated with 10 µg ultra-leaf anti-CD86 antibody (clone IT2.2) or mouse IgG2a isotype control (clone: MOPC-21). After 5 days, BMO were collected and either analyzed with confocal imaging (see below) or dissociated with a mixture of Dispase II, Liberase TL and DNAse at 37°C for 25 minutes. After incubation, single cell suspensions were washed with a FACS staining buffer containing protein and then analyzed by flow cytometry as described above.

Immunofluorescent staining of whole BMOs

BMOs were fixed with 4 % paraformaldehyde for 1 hour at room temperature (RT). After fixation, they were permeabilized in a blocking buffer (3 % FBS, 1 % BSA, 0.5 % Triton X-100, 0.5 % Tween 20, 0.01 % sodium deoxycholate) for 3 hours at RT on a shaker. The BMOs were then incubated overnight at 4°C with a primary antibody (anti-NGFR/CD271, 1:500) in blocking buffer. After three 10-minute washes with PBST (0.05 % Tween in PBS), they were incubated with a secondary antibody (AlexaFluor

568, 1:300) for 2 hours at RT. The BMOs were washed three more times with PBST, mounted in a 1.0 mm iSpacer on a 22x50mm no. 1.5 coverslip, sealed with double-sided tape, and stored in the dark at 4°C until imaging.

Confocal imaging

Confocal laser scanning microscopy (CLSM) of the whole organoids was conducted using an inverted Leica SP8 3X microscope, which features a tunable white light laser and hybrid diode detectors. The microscope is equipped with a 25x/NA0.95-Leica water immersion objective and optical zoom was employed for further magnification. To capture images, spectral channels were taken in sequence and adjusted to optimally excite the fluorophores, while minimizing bleed-through and background noise. The Nyquist criterion was applied to determine the appropriate voxel size for x-y-z series acquisition, ensuring accurate sampling for the applied hardware settings. Additionally, tile scans were performed to comprehensively capture entire organoids using the Leica Navigator function. Image acquisition was achieved through LASX (v.3.8) and deconvolution was performed with the fully integrated Leica lightening software plugin using standard settings. Subsequent image processing was done in Imaris (v.10.0).

CRISPR/Cas9-mediated generation of knockout cell lines

L-428-CD30$^{-/-}$ or KM-H2-CD86$^{-/-}$ cells were generated as previously described [14]. In brief, a two-component guide RNA (gRNA) method was used, and tumor cells were pulsed (pulse code – EW-106) using a 4D-Nucleofector (Lonza, Switzerland). gRNAs (for CD30 C12: GTGTGAGCCCGACTACTACC; C03: TCGACATTCGCAGGTGCGGG; for CD86 Hs.Cas9.CD86.1.AA: GTAACCGTGTATAGATGAGC, Hs.Cas9.CD86.1.AK: CAAGTTTTGATTCGGACAGT, hCD86_C10: TATGACCATCT) were designed and selected from CHOPCHOPv3[23] and subsequently synthesized at IDT (Integrated DNA technologies). Successful knockout of CD30 or CD86 was verified by flow cytometry. CD30 or CD86-negative cells were sorted using a BD FACSAria™ III cell sorter. Polyclonally sorted L-428-CD30$^{-/-}$ or KM-H2-CD86$^{-/-}$ single cell clones were used for all subsequent experiments.

Proliferation assay with cHL tumor cells and blocking antibodies

Human cHL cell lines L-540, L-428 or KM-H2 transduced with a fLuc plasmid were treated with 1 µg ultra-leaf anti-CD86 antibody (clone IT2.2) or mouse IgG2a isotype control (clone: MOPC-21). 50.000 cells were then plated into each well of a 96-well flat bottom plate coated with poly-L-Lysine. Tumor proliferation was measured using Sartorius Incucyte® S3. Cell segmentation and analyses was performed with Incucyte® S3 Software 2022B, Rev2 according to the instructions provided by the manufacturer.

Generation of *in vitro*-polarized macrophages and co-cultures

In vitro-polarized macrophages were generated as follows: PBMC were isolated from healthy donors. $CD14^+$ monocytes were enriched using MACS (Miltenyi Biotec, Germany) according to manufacture's instruction. $CD14^+$ cells were then differentiated into M_1 (10 ng/ml GM-CSF) or M_2 and M_h (50 ng/ml M-CSF) trajectories for seven days. Fresh cytokines were supplemented after three days. After seven days, macrophages were polarized for 24 hours with either 100 ng/ml LPS and 10 ng/ml IFNγ (M_1), 20 ng/ml IL-4 and 20 ng/ml IL-13 (M_2) or with cell-free tumor supernatant of L-428 cHL cells M_h. After 24 hours, macrophages were phenotyped using the above described antibodies to ensure successful generation and polarization and subsequently used for co-culture experiments.

Following polarization towards M_1, M_2 or M_h trajectories, macrophages were stained with a CellTrace™ Violet Proliferation Dye (CTV, Thermo Fisher Scientific, USA). CTV+ macrophages were then co-cultured with CD86-28z, CD30-28z or CD19-28z labeled with a CellTrace™ FarRed Proliferation Dye (CTR, Thermo Fisher Scientific, USA) for two to seven days at an E:T ratio of 1:1. After the co-culture period, the experiment was analyzed by flow cytometry.

Cytotoxicity assays

To determine killing efficiencies of CAR T cells, first, 30.000 – 50.000 cHL, NHL, J774A.1 or control cell lines were seeded in a flat-bottom 96-well plate. Then, different numbers of CAR T cells (at indicated E:T ratios) were added to the wells. The killing of tumor cells was determined by bioluminescence measurement (Bio-Glo™ Luciferase Assay System, Promega Corporation, USA) or flow cytometry. Normalization to control conditions was carried out to determine specific lysis of tumor cells.

Proliferation assays with T cells

To determine T cell proliferation, T cells were stained with a CellTrace™ Far Red Cell Proliferation Kit (ThermoFisher Scientific, USA) before co-culturing with tumor cells. Proliferation was then determined by trace dilution after seven days of co-culture. Proliferation assays of CAR T cells and tumor cells were performed at an E:T ratio of 0.5:1, co-cultures of CAR T cells and *in vitro*-polarized macrophages at an E:T ratio of 1:1.

Cytokine measurements

Cytokine release or percentage of cytokine-positive T cells were determined either by ELISA of co-culture supernatants or flow cytometric analysis of the T cells. The following ELISA kit was used according to the manufacture's instruction: IFNγ, BD Bioscience. Non-detectable (n.d.) was measured at the lowest dilution of 1 to 10. Values marked as "delta" were subtracted from the value of the control group (T cell-only control).

Figure Legends

Supplemental Figure 1: Identification of CD80, CD86 and PD-L1 as potential therapeutic targets in cHL.

(A, B) Heatmaps illustrating the expression of candidate antigens on a panel of cHL (**A**, n = 6;) or NHL cell lines (**B**, n = 3). Microarray data (GSE20011) was obtained from the gene expression omnibus. (**C**) Summary of all data sets used for single-cell cross-organ off-target transcriptomic atlas screening.
cHL, classic Hodgkin lymphoma; NHL, Non-Hodgkin lymphoma.

Supplemental Figure 2: Overview of integration and reclustering of scRNA-seq dataset generated by *Aoki et al.*

(**A**) UMAP plot visualizing the pooled and integrated cHL and RLN samples obtained from *Aoki et al*. (**B**) Dot plot summarizing the distribution of marker genes across different cell clusters. DGE analysis was performed using Wilcoxon test with subsequent Bonferroni p-value adjustment. (**C**) Heatmap visualizing the significantly upregulated functional modules as the result of the DGE analysis between the cell subsets. (**D**) UMAP plots showing combined expression of "proliferative" cell cluster-associated target genes (**left**) or projected cell cycle stated as determined by the CellCycleScoring of the Seurat R package (**right**). (**E**) Distribution of the different disease specimen across the identified immune cell clusters. (**F)** Percentages of cells belonging to the RLN or cHL samples within the identified immune cell subsets, respectively.
cHL, classic Hodgkin lymphoma; RLN, reactive lymph node.

Supplemental Figure 3: CD86 is highly expressed on HRS cells of cHL subtypes.

(A) Summary of all datasets and primary patient material. **(B)** Table summarizing the patient characteristics of cHL specimen used for IHC and multiplexed immunofluorescence. **(C, D)** Expression of CD86 on HRS cells measured by multiplex immunofluorescence microscopy on chip-loaded cHL samples of the nodular sclerosis (NS) subtype (**C)** or mixed cellularity (MC) subtype (**D**). Chips were sequentially stained with antibodies against CD86 (yellow), CD30 (blue), and CD20 (red) and with a DNA Hoechst Stain (blue). Between each staining step, images were acquired with a fluorescence microscope followed by a 30s photobleaching procedure.
HRS cells, Hodgkin-Reed Sternberg cells; cHL, classic Hodgkin lymphoma; NS, Nodular sclerosis; MC, mixed cellularity.

Supplemental Figure 4: CD86 blockade does not influence the proliferation or the phenotype of cHL cell lines.

(A, B) Representative histograms (**A**) and measured mean fluorescence intensity (MFI) (**B**) of the indicated antigen measured by flow cytometry. The experiment is representative of at least two independent measurements. **(C, D)** Representative images (**C**) or quantification of fluorescent intensity (**D**) of cHL cell lines incubated with anti-CD86 blocking antibody (mocha) or isotype control (yellow)

or not treated (grey). Cell proliferation was assessed with live cell imaging. Data are mean ± s.e.m from n = 3 independent experiments. **(E, F)** Representative flow cytometric histograms of CD86 expression of wildtype (WT, top, mocha) or $CD86^{-/-}$-CRISPR-Cas9 (bottom, orange). (**F**) Proliferation of WT or $CD86^{-/-}$ quantified by live cell imaging. Data are mean ± s.e.m from n = 3 independent experiments. (**G**) Overview of experimental scheme used to assess phenotypic changes in cHL cells. (**H**) Heatmaps illustrating expression of hallmark cHL antigens on cHL cell lines L-540 (left), L-428 (middle left), KM-H2 (middle right) or Nalm-6 controls cells (right) measured by flow cytometry. Data are mean from n = 3 independent experiments.

For all panels, statistical significance was calculated using two-way ANOVA with Tukey's or Šidák multiple comparison correction. * $P < 0.05$, ** $P < 0.01$, *** $P < 0.001$, **** $P < 0.0001$, ns $p > 0.05$.

Supplemental Figure 5: CD86 blockade reduces expression inhibitory cell surface markers PD-1 and CTLA-4 on cHL-associated T cells.

(**A, B**) Overview of the experimental scheme used to investigate the impact of CD86 blockade on the cHL-TME (**A**, L-540, L-428, KM-H2) or with Nalm-6 tumor cells (**B**). (**C, D**) Expression of indicated antigens on either $CD14^+$ monocytes (left, CD86) or $CD3^+$ T cells (middle left, CTLA-4; middle right PD-1; right CD28) measured by flow cytometry. KM-H2 (**C**) or Nalm-6 tumor cells (**D**) and PBMC were co-cultured either with αCD86 antibody or isotype control antibody. Data are mean ± s.e.m from n = 6 independent donors. Statistical significance was calculated using Wilcoxon signed-rank test. **(E, F)** Flow cytometric quantification of GFP^+ tumor cells (**E**) or CD28 expression (**F**) in different organs on $CD3^+$ T cell in PBMC-humanized, L-540-tumor-bearing mice. n = 5-6 mice per group. Statistical significance was calculated using two-way ANOVA with Tukey's multiple comparison correction. **(G, H)** Cellular composition of the generated CAR products measured by flow cytometry. Data are mean ± s.e.m of n = 3 different donors. (**G**) T cell subsets. (**H**) Measured CD4 to CD8 ratio. **(I, J)** Killing of tumor cells (**I**) or proliferation of CAR (**J**) in co-cultures of CD86-28z, CD30-28z or CD19-28z CAR with cHL cell lines or Nalm-6 controls. Killing of tumor cells (**I**) or proliferation of T cells (**J**) was determined by flow cytometry, after gating for GFP^+ cells (tumor cells) or $CD3^+$ cells T cells), respectively. Data are mean ± s.e.m from n = 3 independent donors. Statistical significance was calculated using two-way ANOVA with Šidák multiple comparison correction.

For all panels, * $P < 0.05$, ** $P < 0.01$, *** $P < 0.001$, **** $P < 0.0001$, ns $p > 0.05$.

Supplemental Figure 6: cHL TAM express CD86 and CD86-28z CAR engage *in vitro*-polarized $CD86^+$ TAM.

(A) UMAP visualization of reclustered, cHL-infiltrating macrophages. **(B)** Overall fractions of the identified macrophage subsets in cHL specimen. **(C)** Heat map summarizing the distribution of known characteristic macrophages markers on cHL-TAM. Each column represents a different macrophage cluster (0 – 3). **(D, E**) Heat maps illustrating the expression of M_1- or M_2-associated cytokines on cHL

cell lines (**D**, n = 6) or primary cHL samples (**E**, n = 12). Microarray data (GSE20011) was obtained from the gene expression omnibus. **(F)** The phenotype of $CD14^+$ monocytes differentiated to macrophages and subsequently polarized towards M_1-like (LPS, IFNγ), M_2-like (IL-4, IL-13) or M_H-like (cell-free cHL-tumor supernatant without addition of cytokines) trajectories *in vitro*. **(G)** Representative flow cytometric image of CD86 expression on *in vitro*-polarized macrophages compared to an isotype control. (**H**) Antigen-specific proliferation of FarRed proliferation dye stained CD86-28z CAR T cells (top, mocca), CD30-28z CAR T cells (middle, teal), and CD19-28z CAR T cells (bottom, grey) determined by trace dilution co-cultured with *in vitro*-polarized macrophages. (**I**) Lysis of *in vitro*-polarized macrophages, determined by flow cytometry, by CD86-28z CAR T cells, CD30-28z CAR T cells, and CD19-28z CAR T cells. (**J**) IFNγ release into supernatants of in *vitro* polarized macrophages co-cultured with CD86-28z CAR T cells, CD30-28z CAR T cells, and CD19-28z CAR T cells measured by ELISA. **(F - J)** Data are mean ± s.e.m from n = 6 six different donors. Statistical significance was calculated using two-way ANOVA with Šidák multiple comparison correction.
For all panels, * $P < 0.05$, ** $P < 0.01$, *** $P < 0.001$, **** $P < 0.0001$, ns $p > 0.05$.
n.d. – not detectable

Supplemental Figure 7: CD86-28z CAR remain effective in CD30-negative disease and can control tumor growth in challenging cHL-models *in vivo*.
(A) Representative flow cytometric staining of expression of CD86 (left) or CD30 (right) on generated L-428-$CD30^{-/-}$ cell line. Staining was carried out at least 7 days after completion of the CRISPR-Cas9 protocol. Data is representative of at least two independent experiments. **(B)** L-428-$CD30^{-/-}$ cells were co-cultured with CD86-28z (mocha), CD30-28z (teal) or CD19-28z (grey) CAR, respectively, for 72 h. Tumor cell killing was determined by bioluminescence measurement and specific lysis was calculated after normalization to tumor cell-only controls. **(C)** L-428- WT or -$CD30^{-/-}$ cells were co-cultured with CD30-28z CAR T cells. Representative flow cytometry histograms of intracellular staining of $GzmB^+$ are shown after 12 h of incubation with GolgiStop and GolgiPlug. (**B, C**) Data are mean ± s.e.m from n = 3 different donors. **(D)** Summary of the treatment schedule used for L-428 xenograft *in vivo* experiments. **(E - G)** BLI images (**E**), fLuc-BLI-based quantification of tumor burden (**F**), and Kaplan-Meier estimation of overall survival (**G**) of L-428-tumor bearing mice treated with CD86-28z, CD30-28z or CD19-28z CAR T cells, respectively. Shown is pooled data from two independent experiments of n = 4 – 7 mice per group. **(H)** Summary of the *in vivo* treatment schedule of L-540-based challenge models *in vivo*. **(I - K)** BLI images (**I**) fLuc-BLI-based quantification of tumor burden (**J**) or overall survival (**K**) of L-540-tumor bearing mice, treated with CD86-28z, CD30-28z or CD19-28z CAR T cells. n = 5 mice per group. **(L)** Representative flow cytometric image of CD19-28z-teLuc or CD86-28z-teLuc double-transduced cells. Data is representative of at least three independent donors.
For all panels, statistical significance was calculated using two-way ANOVA with Šidák multiple comparison correction. For Kaplan-Meier-curves, statistical significance was calculated with a log-rank test. * $P < 0.05$, ** $P < 0.01$, *** $P < 0.001$, **** $P < 0.0001$, ns $p > 0.05$.

Supplemental Figure 8: Murine surrogate mCD86 CAR T cells do not cause measurable toxicity in syngeneic mouse models.

(A) Summary of the composition of anti-murine CD86 (mCD86-28z) or anti-murine EpCAM CAR (mEpCAM-28z) constructs. **(B)** Representative flow cytometric images of transduction efficiencies of primary murine T cells. Efficiencies measured by flow cytometric measurement of GFP-positive cells. **(C)** Percentage $CD69^+$ (**left**) or $CD107a^+$ (**right**) mCD86-28z (mocha), mEpCAM-CD28z (grey) or untransduced T cells (UT, green) after incubation with Fc-immobilized mCD86 protein. Data are mean ± s.e.m of six biological replicates. Shown is one representative of n = 3 independent experiments. **(D, E)** Representative flow cytometric images (**D**) or geometric MFI (**E**) of mCD86 expression on J77A4.1 cells. **(F, G)** CD86-28z (mocha), mEpCAM-CD28z (grey) CAR T cells or UT (green) were co-cultured J774A.1 for 48h at the indicated T cell to Tumor cell ratios. **(F)** Lysis was determined by bioluminescent measurements. (**G**) Secretion of mIFNγ measured by ELISA. Data are mean ± s.e.m from n = 3 independent experiments. (**H**) Summary of the treatment schedule used for toxicity assessment in C57Bl/6 mice. (**I**) Weight curves of mice treated with mCD86 CAR T cells or GFP control cells (n = 5 mice per group). (**J - L**) Percentage of transferred T cells (**J**) or indicated cell type (**K**) in the blood of C57Bl/6 mice 8 days after ACT or after sacrificing the mice at day 29 (**L**). (**M**) Percentage of transferred T cells in the blood of C57Bl/6 mice at indicated time points after ACT measured by flow cytometry in s.c. OVA vaccination model or percentage of $CD86^+$ B cells in the blood (**N**). (**O, P)** Percentage of transferred T cells in the blood of C57Bl/6 mice in polymicrobial sepsis model at indicated time points after ACT in the blood (**O**) or in the organs after sacrificing the mice (**P**) measured by flow cytometry. (**Q**) Percentage of $CD86^+$ B cells in the organs of C57Bl/6 mice after sacrifice.

For all panels, data are mean ± s.e.m of the indicated n number. Statistical significance was calculated using two-way ANOVA with Šidák or Tukey's multiple comparison correction or unpaired t-test. For Kaplan-Meier-Curves, statistical significance was calculated with log-rank test.

* $P < 0.05$, ** $P < 0.01$, *** $P < 0.001$, **** $P < 0.0001$, ns $p > 0.05$.

References

[1] Brune V, Tiacci E, Pfeil I, Doring C, Eckerle S, van Noesel CJ, et al. Origin and pathogenesis of nodular lymphocyte-predominant Hodgkin lymphoma as revealed by global gene expression analysis. J Exp Med. 2008;205:2251-68.

[2] Aoki T, Chong LC, Takata K, Milne K, Hav M, Colombo A, et al. Single-Cell Transcriptome Analysis Reveals Disease-Defining T-cell Subsets in the Tumor Microenvironment of Classic Hodgkin Lymphoma. Cancer Discov. 2020;10:406-21.

[3] Stuart T, Butler A, Hoffman P, Hafemeister C, Papalexi E, Mauck WM, 3rd, et al. Comprehensive Integration of Single-Cell Data. Cell. 2019;177:1888-902 e21.

[4] Chen L, Flies DB. Molecular mechanisms of T cell co-stimulation and co-inhibition. Nat Rev Immunol. 2013;13:227-42.

[5] Wolf FA, Angerer P, Theis FJ. SCANPY: large-scale single-cell gene expression data analysis. Genome Biol. 2018;19:15.

[6] Virshup I, Rybakov S, Theis FJ, Angerer P, Wolf FA. anndata: Annotated data. bioRxiv. 2021:2021.12.16.473007.

[7] Fischer DS, Dony L, Konig M, Moeed A, Zappia L, Heumos L, et al. Sfaira accelerates data and model reuse in single cell genomics. Genome Biol. 2021;22:248.

[8] Lun AT, Bach K, Marioni JC. Pooling across cells to normalize single-cell RNA sequencing data with many zero counts. Genome Biol. 2016;17:75.

[9] Lun AT, McCarthy DJ, Marioni JC. A step-by-step workflow for low-level analysis of single-cell RNA-seq data with Bioconductor. F1000Res. 2016;5:2122.

[10] Sandhofer N, Metzeler KH, Rothenberg M, Herold T, Tiedt S, Groiss V, et al. Dual PI3K/mTOR inhibition shows antileukemic activity in MLL-rearranged acute myeloid leukemia. Leukemia. 2015;29:828-38.

[11] Yeh HW, Karmach O, Ji A, Carter D, Martins-Green MM, Ai HW. Red-shifted luciferase-luciferin pairs for enhanced bioluminescence imaging. Nat Methods. 2017;14:971-4.

[12] Starr ME, Steele AM, Saito M, Hacker BJ, Evers BM, Saito H. A new cecal slurry preparation protocol with improved long-term reproducibility for animal models of sepsis. PLoS One. 2014;9:e115705.

[13] Lesch S, Blumenberg V, Stoiber S, Gottschlich A, Ogonek J, Cadilha BL, et al. T cells armed with C-X-C chemokine receptor type 6 enhance adoptive cell therapy for pancreatic tumours. Nature Biomedical Engineering. 2021.

[14] Cadilha BL, Benmebarek M-R, Dorman K, Oner A, Lorenzini T, Obeck H, et al. Combined tumor-directed recruitment and protection from immune suppression enable CAR T cell efficacy in solid tumors. Science Advances. 2021;7:eabi5781.

[15] Kobold S, Grassmann S, Chaloupka M, Lampert C, Wenk S, Kraus F, et al. Impact of a New Fusion Receptor on PD-1-Mediated Immunosuppression in Adoptive T Cell Therapy. J Natl Cancer Inst. 2015;107.

[16] Benmebarek MR, Cadilha BL, Herrmann M, Lesch S, Schmitt S, Stoiber S, et al. A modular and controllable T cell therapy platform for acute myeloid leukemia. Leukemia. 2021.

[17] Ghani K, Wang X, de Campos-Lima PO, Olszewska M, Kamen A, Riviere I, et al. Efficient human hematopoietic cell transduction using RD114- and GALV-pseudotyped retroviral vectors produced in suspension and serum-free media. Hum Gene Ther. 2009;20:966-74.

[18] Karches CH, Benmebarek MR, Schmidbauer ML, Kurzay M, Klaus R, Geiger M, et al. Bispecific Antibodies Enable Synthetic Agonistic Receptor-Transduced T Cells for Tumor Immunotherapy. Clin Cancer Res. 2019;25:5890-900.

[19] Brockelmann PJ, Buhnen I, Meissner J, Trautmann-Grill K, Herhaus P, Halbsguth TV, et al. Nivolumab and Doxorubicin, Vinblastine, and Dacarbazine in Early-Stage Unfavorable

Hodgkin Lymphoma: Final Analysis of the Randomized German Hodgkin Study Group Phase II NIVAHL Trial. J Clin Oncol. 2023;41:1193-9.
[20] Reinke S, Brockelmann PJ, Iaccarino I, Garcia-Marquez M, Borchmann S, Jochims F, et al. Tumor and microenvironment response but no cytotoxic T-cell activation in classic Hodgkin lymphoma treated with anti-PD1. Blood. 2020;136:2851-63.
[21] Jarosch S, Kohlen J, Wagner S, D'Ippolito E, Busch DH. ChipCytometry for multiplexed detection of protein and mRNA markers on human FFPE tissue samples. STAR Protoc. 2022;3:101374.
[22] Frenz-Wiessner S, Fairley SD, Buser M, Goek I, Salewskij K, Jonsson G, et al. Generation of complex bone marrow organoids from human induced pluripotent stem cells. Nat Methods. 2024;21:868-81.
[23] Labun K, Montague TG, Krause M, Torres Cleuren YN, Tjeldnes H, Valen E. CHOPCHOP v3: expanding the CRISPR web toolbox beyond genome editing. Nucleic Acids Res. 2019;47:W171-W4.

Supplemental Figure 1

A

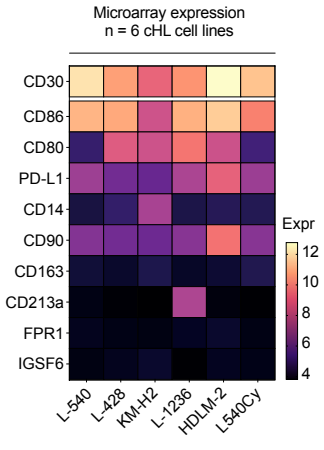

B

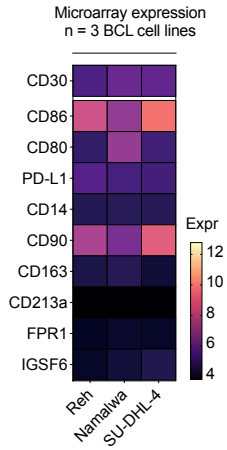

C

Organ	Method	n (donors)	n (cells)	Publication
GI	10X	6	79267	Madissoon et al., 2019
	microwell-seq	2	11313	Han et al., 2020
	10X	5	41640	James et al., 2020
	10X 3' v2	17	149250	Fawkner-Corbett et al., 2021
	10X	2	3624	Wang et al., 2020
	10X 3' v2, smart seq2	2	13657	Tabula Sapiens et al., 2022
Liver	10X 3' v2	1	6271	MacParland et al., 2018
	10X	5	33519	Ramachandran et al., 2019
	10X 3' v2, smart seq2	2	4988	Tabula Sapiens et al., 2022
	10X	4	139136	Andrews et al., 2022
	microwell-seq	3	10549	Han et al., 2020
	10X	12	13138	Suo et al., 2022
Pancreas	Bulk-RNA-Seq	4	8324	Baron et al., 2016
	HiSeqXTen	11	15194	Peng et al., 2019
	Smart-seq2	9	2468	Enge et al., 2017
	CEL-seq2	4	2126	van den Brink et al., 2017
	10X 3' v2, smart seq2	2	13488	Tabula Sapiens et al., 2022
	microwell-seq	1	9701	Han et al., 2020
Kidney	10X	1	37422	Stewart et al., 2019
	10X 5' v1	5	19982	Muto et al., 2021
	10X 3' v3, smart seq2	1	9634	Tabula Sapiens et al., 2022
	microwell-seq	3	22929	Han et al., 2020
Skin	10X	9	68036	Cheng et al., 2018
	10X 3' v3, smart seq2	2	9422	Tabula Sapiens et al., 2022
Lymph Node	10X, Illumina HiSeq 2500	12	37439	Kim et al., 2020
	10X 3' v2	1	4355	Xiang et al., 2020
	10X 3' v3, smart seq2	3	53275	Tabula Sapiens et al., 2022
	10X	12	85358	Suo et al., 2022
Brain	DroNc-Seq	1	13067	Habib et al., 2017
	microwell-seq	1	7305	Han et al., 2020
	microwell-seq	1	9520	Han et al., 2020
Lung	10X	3	60633	Travaglini et al., 2020
	10X	5	56304	Madissoon et al., 2019
	Bulk-RNA-Seq	8	41503	Reyfman et al., 2019
	10X, Illumina HiSeq 2500	11	36334	Kim et al., 2020
	10X 3' v3, smart seq2	3	35654	Tabula Sapiens et al., 2022
	microwell-seq	3	23999	Han et al., 2020
	10X	12	33870	Suo et al., 2022
Heart	microwell-seq	2	2781	Han et al., 2020
	10X	14	937202	Litviňuková et al., 2020
	10X 3' v3, smart seq2	1	11505	Tabula Sapiens et al., 2022
Blood	10X 3' v3, smart seq2	6	49779	Tabula Sapiens et al., 2022
	microwell-seq	3	12023	Han et al., 2020
	10X	12	27323	Suo et al., 2022
Bone Marrow	nanowell-seq	5	7651	van Galen et al., 2019
	10X 3' v3, smart seq2	4	12291	Tabula Sapiens et al., 2022
	microwell-seq	2	8667	Han et al., 2020
	10X	12	38069	Suo et al., 2022
Spleen	10X 3' v3, smart seq2	3	33941	Tabula Sapiens et al., 2022
	microwell-seq	1	15781	Han et al., 2020
	10X	12	71219	Suo et al., 2022

Supplemental Figure 2

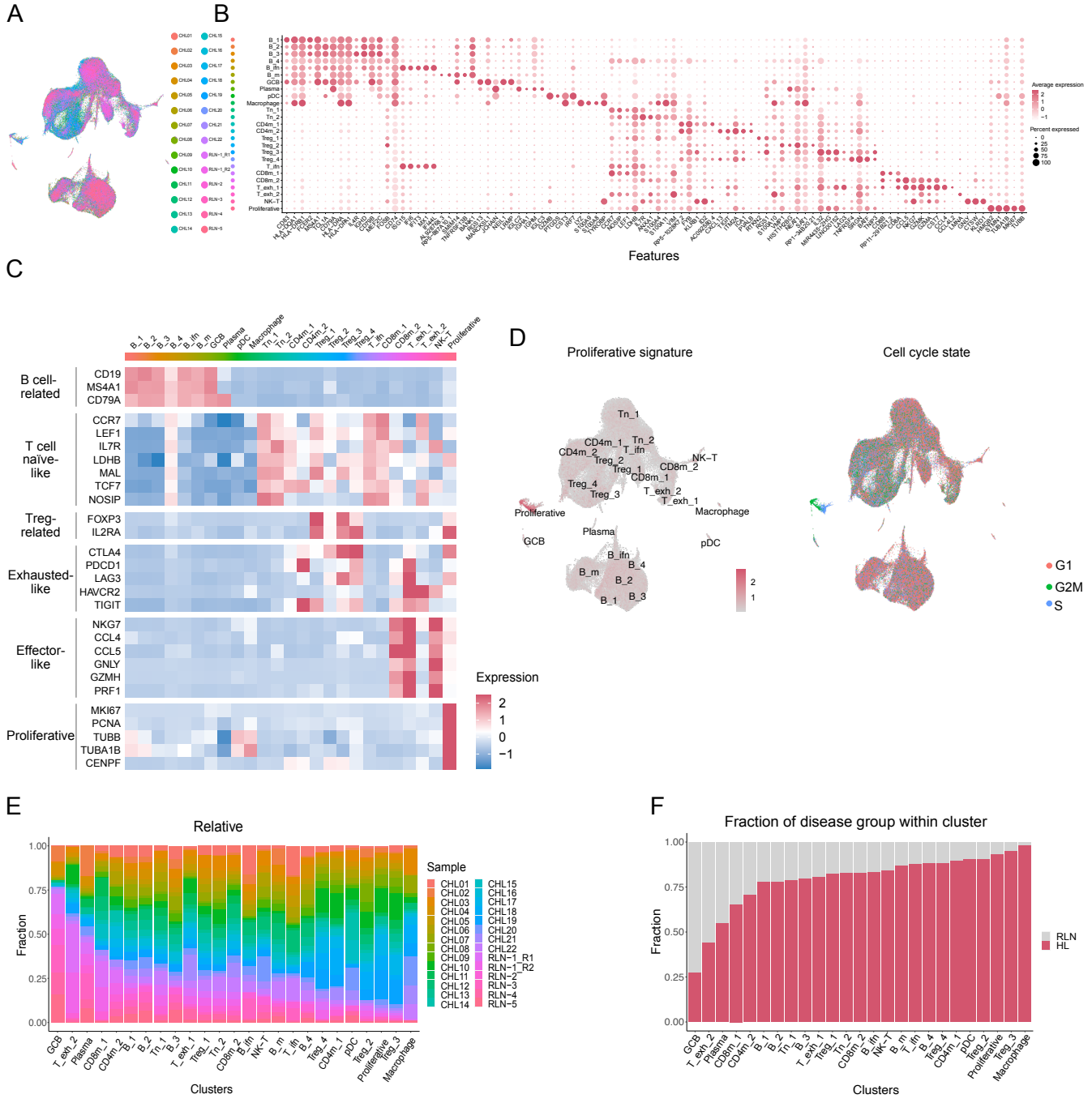

Supplemental Figure 3

A

Origin	Method	cHL	Control	Accessibility
Cell line	Microarray profiling HRS cell lines	6	3	GSE20011
Cell line	Flow cytometric staining	3	1	Not applicable
Origin	**Method**	**cHL**	**RLN**	**Accessibility**
Primary patient samples	Microarray profiling HRS cells	12	5	GSE12453
Primary patient samples	ScRNA-Seq	22	5	EGAS00001005541
Primary patient samples	NIVAHL NanoString profiling	95		Request
Primary patient samples	NIVAHL - Secondary biopsies NanoString profiling	12		Request
Primary patient samples	Immunohistochemistry & multiplex immunofluorescence	21		Not applicable
Summary patient count		**150**	**10**	

B

Sample type	Chip-ID	Age	Sex	Subtype	Method
Primary samples (n = 7)	M2092625	51	female	NS	IHC & Multiplex
	M2099672	66	male	MC	IHC & Multiplex
		75	male	NS	IHC
	M2099674	38	female	MC	IHC & Multiplex
		73	female	MC	IHC
	M2092623	13	female	MC	IHC & Multiplex
		40	male	MC	IHC
Primary samples (n = 4)	M2013957	52	female	NS	Multiplex
	M1353669	33	female	NS	Multiplex
	M1353667	74	male	MC	Multiplex
	M1325296	37	male	MC	Multiplex
Relapsed samples (n = 10)		53	male	MC	IHC
		45	male	MC	IHC
		42	male	NS	IHC
		61	female	NS	IHC
		25	male	NS	IHC
	M2099664	16	male	NS	IHC & Multiplex
		43	female	NS	IHC
		38	male	MC	IHC
		56	male	LR	IHC
		73	female	MC	IHC

C

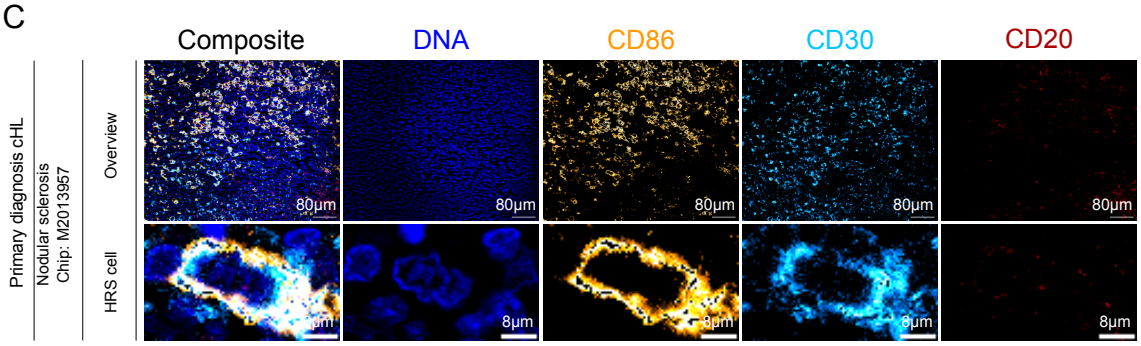

D

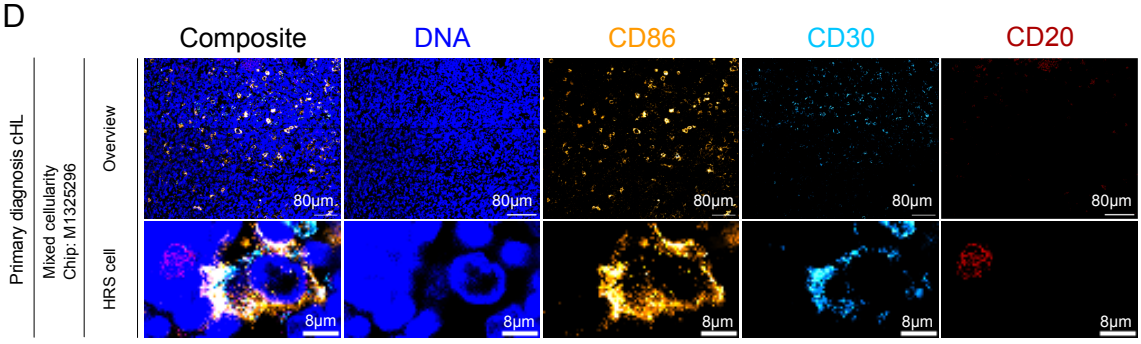

Supplemental Figure 4

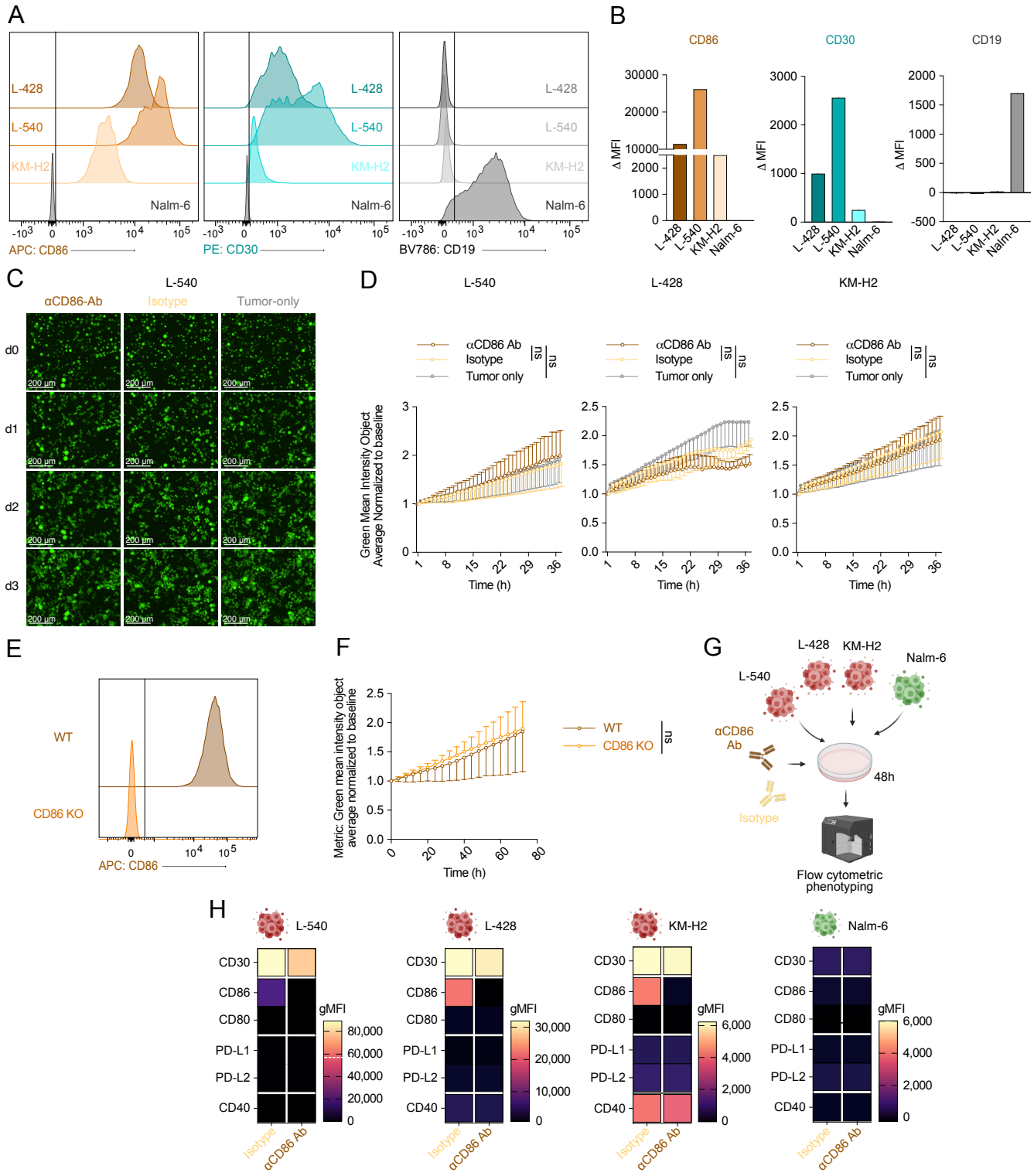

Supplemental Figure 5

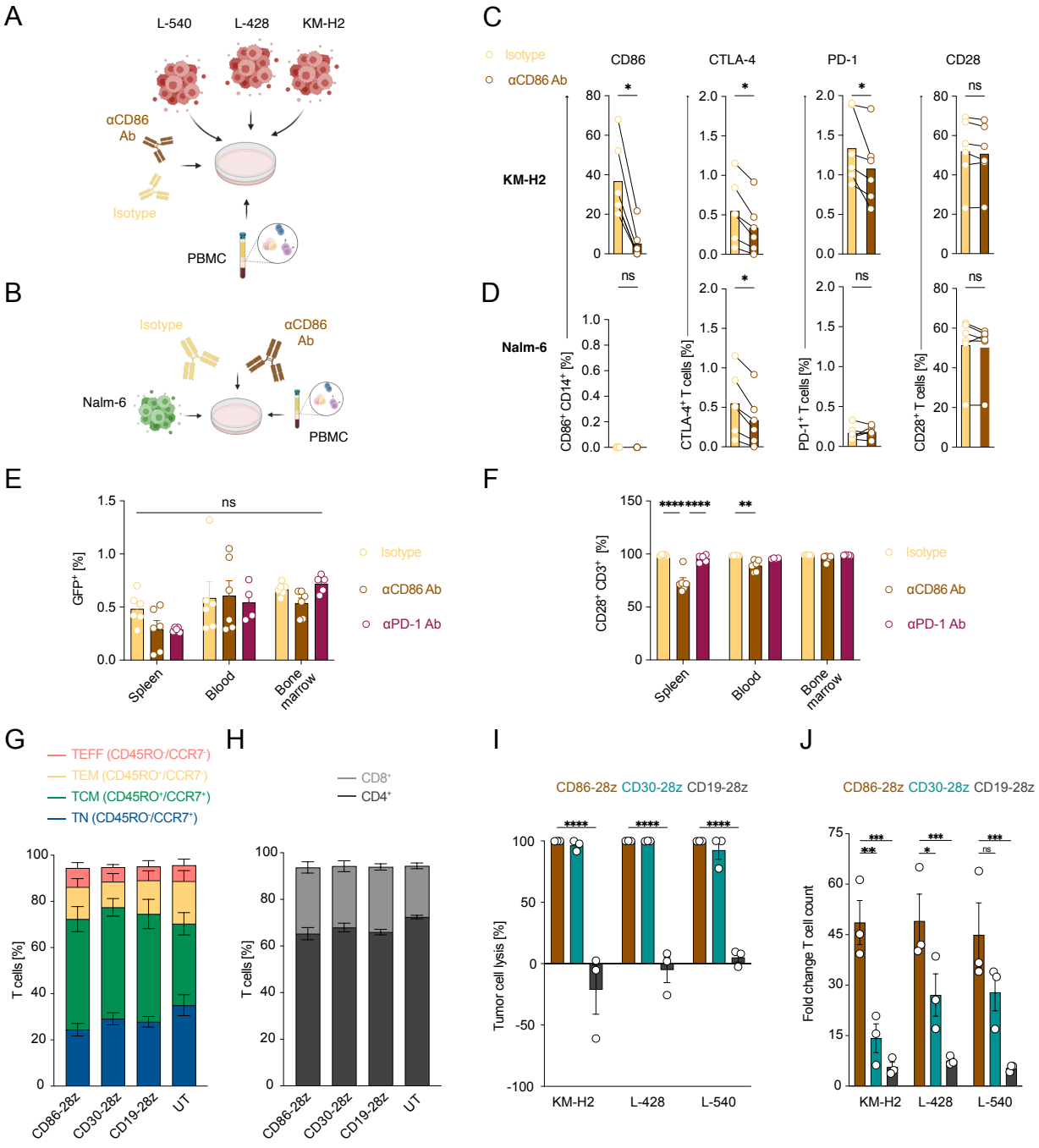

Supplemental Figure 6

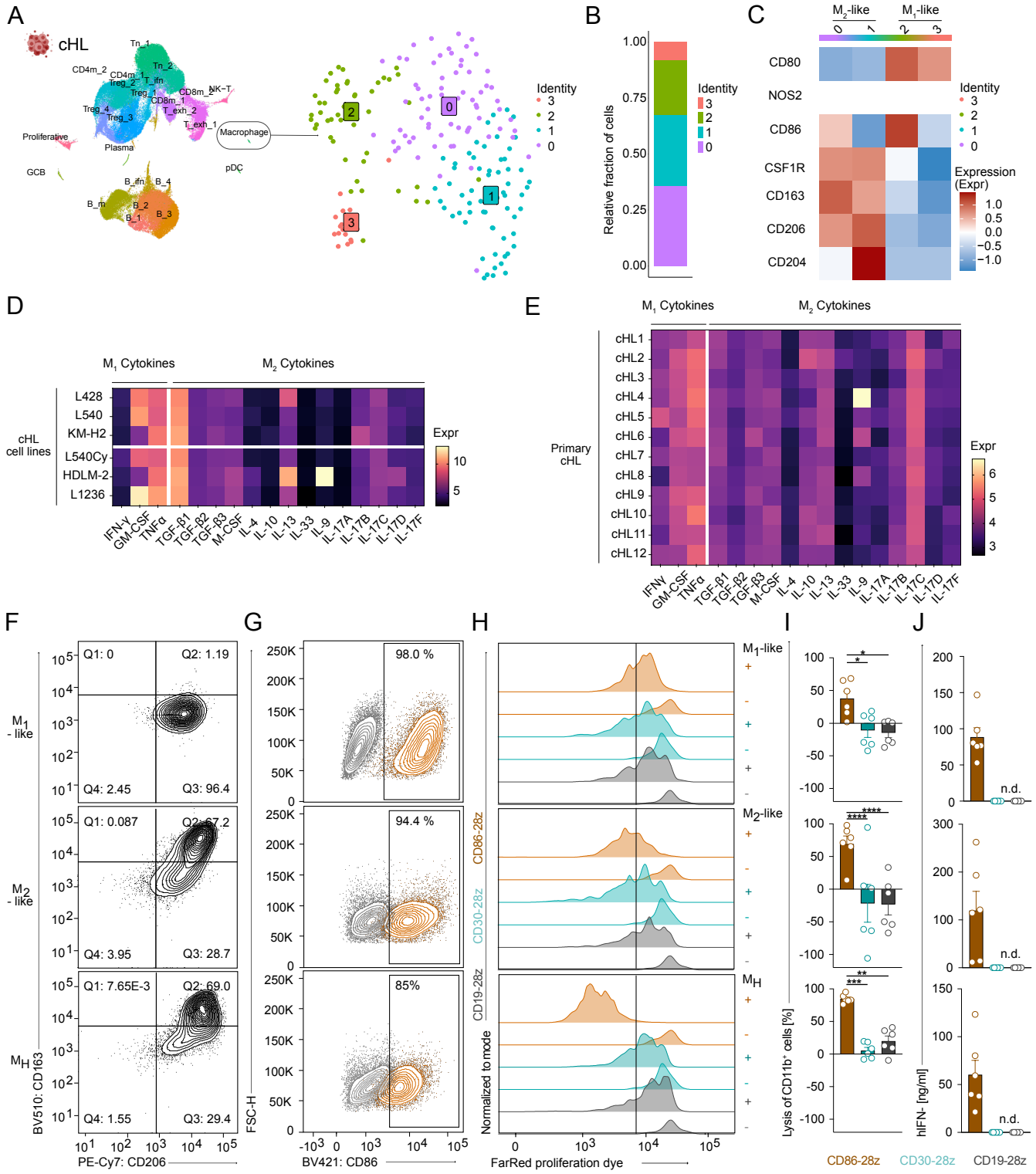

Supplemental Figure 7

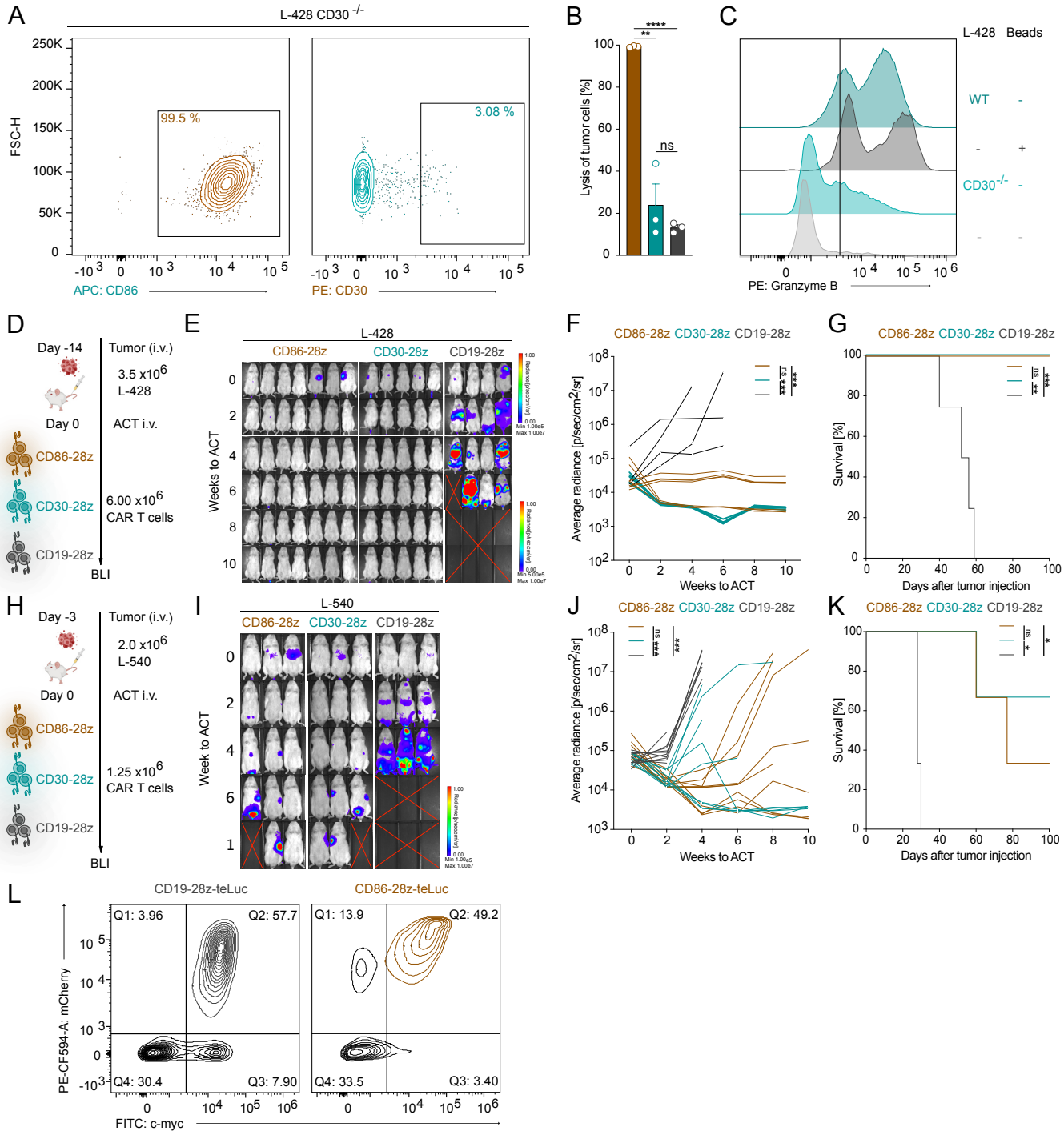

Supplemental Figure 8